Comparison of a MEMS Microactuator and a PZT Milliactuator for High-bandwidth HDD Servo

Matthew T. White*, Pushkar Hingwe#, and Toshiki Hirano*
Hitachi Global Storage Technologies
*San Jose Research Center, 650 Harry Road, San Jose, California 95120, USA
#Advanced Technology, 5600 Cottle Road, San Jose, California 95193, USA
Matthew.White@hgst.com

Abstract—**A microactuator that moves the slider of a hard disk drive (HDD) was fabricated using MEMS techniques. A suspension-mounted PZT milliactuator was also manufactured. Both actuators were assembled and tested in 10,000 RPM server-class HDDs. The MEMS microactuator has a resonance at 2.2 kHz that can be controlled by feedback, and has virtually no other modes up to 100 kHz. The first mode of the PZT milliactuator is much higher at 8 kHz, but there are many more modes below 100 kHz. Both secondary actuators enable high tracking servo bandwidth, which is necessary to achieve ultra-high track densities. However, the differences in their mechanics require different control strategies, place different limitations on their performance, and have different effects on the use of their limited stroke. Data on assembly, simulations, and drive-level experiments are presented. Challenges that dual-stage actuators will continue to face are also discussed.**

I. INTRODUCTION

In an ongoing effort to increase storage capacity while decreasing the number of magnetic components and manufacturing cost, hard disk drive companies have aggressively increased the number of data tracks per inch that are stored on the magnetic media. This has placed tighter requirements on the servo system that controls the position of the magnetic read/write heads with respect to the data tracks. Current disk drive designs use a single rotary actuator with a voice coil motor (VCM) at one end of the actuator arm, the magnetic read/write heads at the other end, and a pivot bearing in between. The position information used for control is encoded on the disks and read by the magnetic read head, resulting in a non-collocated system. The actuator arm is fairly light and flexible, so the dynamics between the VCM and the heads, as well as the VCM pivot friction, are significant. These dynamics limit the servo bandwidth, and consequently the speed at which data tracks can be accessed and the accuracy at which they can be followed.

In the past, advances have been achieved through optimization of the mechanics and the controller design, but the potential to improve these areas with a single stage actuator is decreasing. Secondary actuators, which are placed closer to the read/write heads and move less mass, offer better mechanics and faster response. There are many choices of location and actuation for the secondary actuator, but two of the most popular are a MEMS device placed between the actuator suspension and the slider that carries the read/write heads, and a piezoelectric device that is placed on the suspension. Both have advantages over the single-stage design, and both have challenges that have delayed their implementation into products.

II. DEVICE DESCRIPTIONS

While both secondary actuators have distinct advantages over the standard VCM, they do introduce dynamics to the mechanical design. Also, both require relatively large voltages to generate enough stroke. The typical power supply for desktop and server–class HDDs is 0-5 V and 0-12 V. This voltage can be increased by DC-DC converters and charge pumps, but safety standards limit the maximum voltage. The stroke requirements for the secondary actuator can generally be broken down into the track misregistration (TMR) of the VCM, the inefficiency of the coordination between the VCM and the secondary actuator, and a component for seeks and settling. Particularly for server-class drives, external disturbance rejection influences the stroke requirements.

A. Moving-slider MEMS Microactuator

An SEM of the MEMS microactuator is shown in Fig. 1. It is positioned almost directly over the read/write heads, resulting in a nearly collocated system. The microactuator itself is almost a perfect spring-mass system, so there are few additional dynamics to deal with. A frequency response of the microactuator plant is shown in Fig. 2, compared to the VCM plant that was used for both the microactuator and milliactuator experiments. The spring-mass mode is at 2.2 kHz, and there are no other significant modes below 100 kHz. The device rotates about the fixed axis that can be seen in the center of the device. The resulting lateral motion of the read/write heads is approximately –1.0 μm to 1.0 μm for a driving voltage input of –30 V to +30V. Further details on this device can be found in [1].

Unfortunately, manufacturing these devices can be difficult, and integration into the head and slider assembly is challenging. Issues such as robustness against external particles and transmission of signals between the slider and the suspension must be addressed. They require high stiffness in the vertical direction for the head/disk interface to function properly, but

relatively low stiffness in rotation in order to produce enough displacement for a given voltage. To meet these two requirements, a high-aspect-ratio spring was made, whose typical dimension is 35 μm high and 3 μm wide.

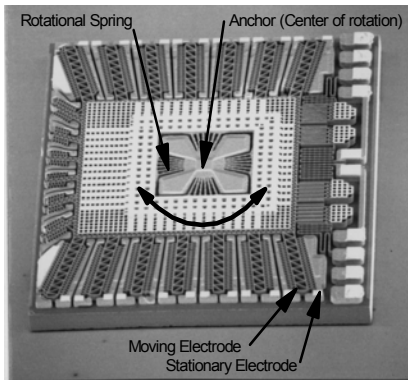

Fig. 1: SEM of the microactuator

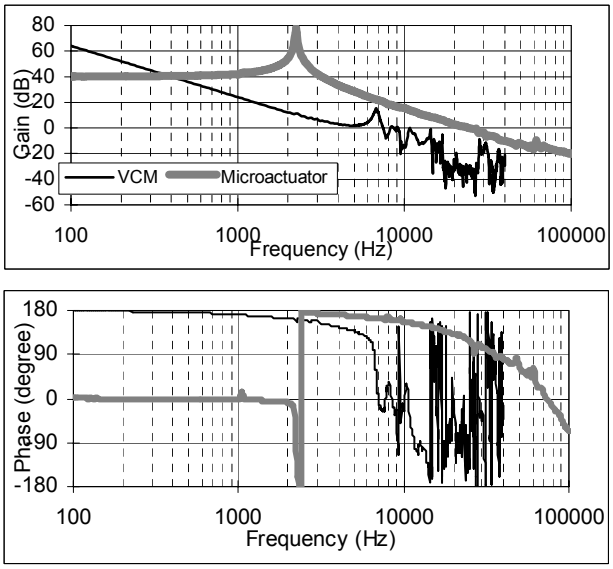

Fig. 2: Plant frequency responses of the microactuator and VCM

B. Suspension-mounted PZT Milliactuator

The milliactuator has two PZT strips that are mounted on a hinge on the suspension. See [2] for a detailed description of a previous generation milliactuator. When voltage is applied, one of the PZTs expands and the other contracts, which causes the suspension to bend in the lateral direction, as shown in Fig. 3. Because the secondary actuator is farther from the complicated assembly of the slider and read/write heads, it is much easier to integrate and manufacture and requires fewer changes to the existing system. However, its positioning means that there are still arm dynamics to contend with. A frequency response of the milliactuator is shown in Fig. 4. The response is flat until the effects of the resonance at approximately 8 kHz, but has several additional modes between 10 kHz and 40 kHz. The stroke of the milliactuator is approximately 1 μm for an input voltage of 25 V. There is a compromise between the stroke (related to the compliance of the suspension relative to the arm) and the first significant mode of the actuated suspension.

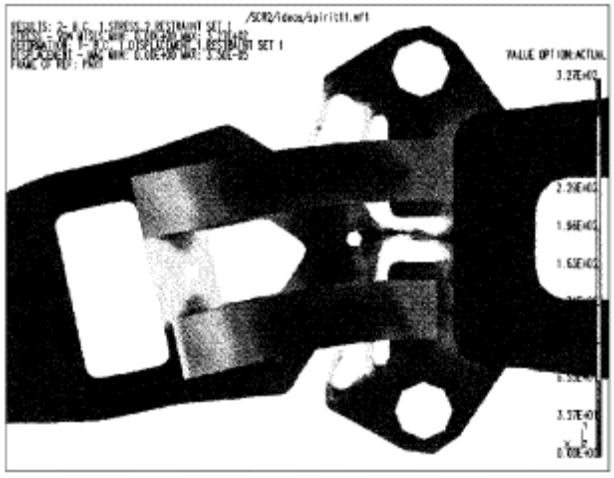

Fig. 3: Detail of the milliactuator bending motion

C. Device Comparison

An important difference between the milliactuator and the microactuator from the controller design point of view is that the milliactuator has relatively little phase loss until the first fundamental mode. Most of the phase loss seen in Fig. 4 before 8 kHz is due to delays in the measurement system. The microactuator, on the other hand, needs considerable phase lead for the phase to be greater than -180 degrees at the bandwidth frequencies. In the milliactuator, the phase advantage is lost because of the need to notch the higher frequency dynamics. Another important difference is the available stroke per volt of actuation. Milliactuator motion per volt is a constant for frequencies up to 8 kHz. For the microactuator, the motion per volt drops of as a square of the frequency for frequencies above its typical main resonance at about 3 kHz. Consequently, the amount of voltage required to move the microactuator at frequencies past its resonance keeps increasing as s^2. If significant TMR benefits are to be had beyond the frequency of the microactuator main resonance, then the milliactuator may have an advantage over the microactuator in terms of voltage actuation required.

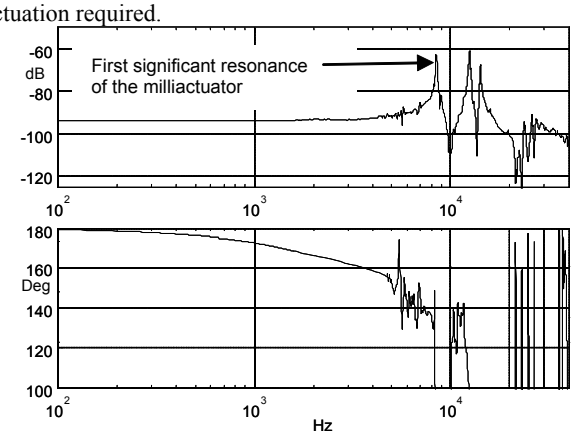

Fig. 4: Milliactuator plant frequency response

The differences in the dynamics of the two devices dictate different controller design strategies. Dual-stage designs using the milliactuator generally place the open loop bandwidth before the main resonance of the milliactuator of about 8 kHz. The open loop bandwidth of the microactuator designs are generally placed between the first resonance at about 3 kHz and the higher frequency resonances starting at about 100 kHz. Consequently, the microactuator is generally able to achieve higher bandwidth. However, the microactuator controller must accommodate the resonance in the 3 kHz region, which may place limitations on the design. The milliactuator design generally has more freedom in the frequency range, which may lead to improved rejection of disturbances.

III. TRACK-FOLLOWING CONTROLLER STRUCTURE

The general philosophy for maintaining the desired position with respect to the data track is sometimes referred to as the woofer/tweeter approach. The VCM controls the large-amplitude, low-frequency motions and the secondary actuator controls the small-amplitude, high-frequency motions. Most of the design problems occur in the mid-frequency (handoff) range where the open loop magnitudes are nearly equal. If the phases in this region are close to 180 degrees apart, the two devices interfere destructively, leading to degraded performance and wasted stroke of the secondary actuator. The design of the handoff between the two actuators is very important to minimize destructive interference between them and ensure that the stroke of the secondary actuator is not saturated. Analytical techniques to improve the handoff between the VCM and microactuator loops have been developed [3]. Use of the relative position signal, which is the displacement of the microactuator from its nominal position, may also lead to improved handoff [4].

Typically, the relative position between the VCM and the secondary actuator is unknown. In this case, only the position of the read/write heads is available as a feedback signal, resulting in a dual-input, single-output (DISO) plant. The closed loop transfer function of the parallel configuration shows that the designs of the secondary actuator and VCM loops are coupled:

$$\frac{y}{r} = \frac{C_{MA}P_{MA} + C_{VCM}P_{VCM}}{1 + C_{MA}P_{MA} + C_{VCM}P_{VCM}}. \qquad (1)$$

DISO systems are a subset of MIMO (multi-input, multi-output), and researchers have applied MIMO techniques to the HDD dual-stage control problem [5]. Capacitive sensing can be used on a MEMS device to measure the relative position, but it does increase the complexity and expense. It is also possible to use observers/estimators to predict the relative position, but again, control complexity and cost may be problems for product implementation. If the relative position is available, it is possible to decouple the two control problems, and actively damp the spring-mass resonance of the MEMS microactuator. Previous studies [4] have shown the potential benefits of also using the relative position signal. For ease of comparison between the two devices, no measured or estimated value of the relative position was used, and the DISO parallel configuration was used for both the milliactuator and the microactuator, as shown in Fig. 5, where C_{VCM} is the VCM controller, C_{MA} is the micro-/milliactuator controller, P_{VCM} is the VCM plant, P_{MA} is the micro-/milliactuator plant, r is the reference position, y is the measured position, and PES is the position error signal.

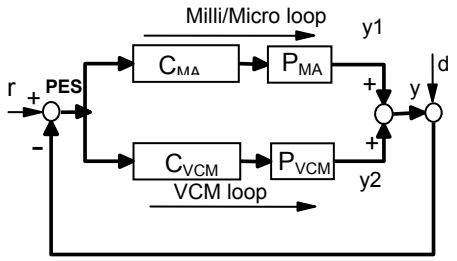

Fig. 5: Parallel feedback configuration

A. Disturbance Effects on Stroke Usage

In product implementation, an important constraint is the stroke of the secondary actuator in different operation environments. From the block diagram in Fig. 5, the stroke is expressed as

$$y1 = d * \frac{C_{MA}P_{MA}}{(1 + C_{MA}P_{MA} + C_{VCM}P_{VCM})} \qquad (2)$$

where y1 is the secondary actuator motion under a position disturbance d. Thus, the stroke of the secondary actuator is directly related to the equivalent position disturbance during the operation of the disk drive. It is also related to the gain of the VCM loop. The higher the gain of the VCM loop is, the lower the secondary actuator stroke is.

As an example, consider a design for a milliactuator. (A discussion of stroke requirements for microactuators may be found in [4].) In Fig. 6, red lines represent VCM-only results and blue lines represent results with the VCM and milliactuator acting together. In the top subplot are the sensitivity functions with and without the milliactuator. A representative disturbance spectrum is given in the middle subplot and includes broadband torque disturbance, external vibrations, and air-flow induced vibrations. The bottom subplot shows the PES spectrum (dotted lines) and the accumulated variance (solid lines) due to the various frequency components of the closed loop PES spectrum. It demonstrates that the milliactuator provides mid-frequency attenuation and a reduction in TMR. This is the typical improvement in TMR that is expected of the milliactuator. The cost of achieving this benefit needs to be weighed against the stroke required during operation under the disturbance.

The top subplot of Fig. 7 shows a representative stroke transfer function, which corresponds to the sensitivity function shown in Fig. 6. The disturbance term of Eqn. 2 is shown in the middle subplot. The bottom subplot shows y1, which is the expected milliactuator motion. Much of the milliactuator stroke is consumed in the low frequency range. This is quite contrary to the range of frequency where the milliactuator loop impacts the

sensitivity function. Given the disturbance and stroke transfer function in Fig. 7, it can be seen that higher VCM loop gain at the low and middle frequencies will relieve the milliactuator of significant stroke usage. One of the strategies to minimize the stroke requirement of the milliactuator is to push the VCM loop gain as high as possible during track follow operation. However, if the VCM loop is to remain stable on its own (in the case that passive protection from milliactuator failure or saturation is desired), then there is a relatively restrictive upper limit on the VCM loop gain, which is related to the VCM loop bandwidth.

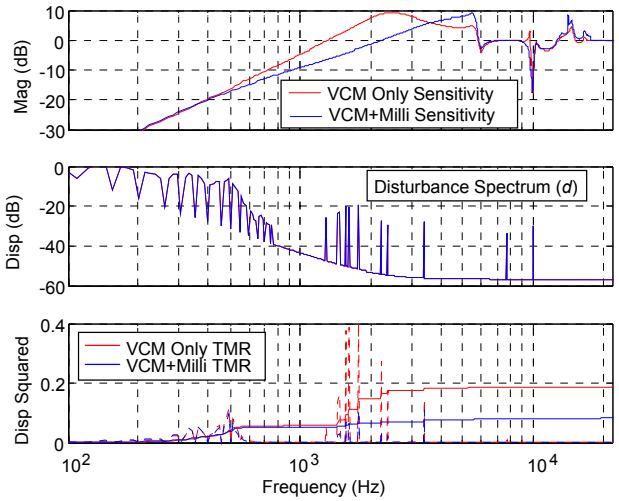

Fig. 6: The typical sensitivity function and TMR impact of the milliactuator

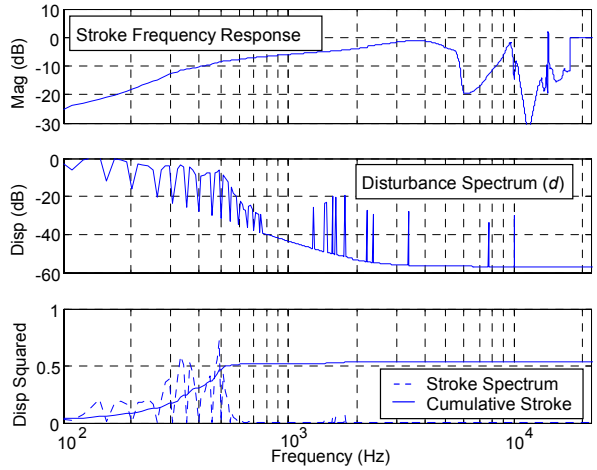

Fig. 7: Typical stroke transfer function and impact of disturbance on the milliactuator stroke

IV. EXPERIMENTAL RESULTS

Both the microactuator and the milliactuator were assembled into 10,000 RPM server-class HDDs. The HDD product card was used for the VCM control and the demodulation of the read/write head position. For the microactuator, the position signal was sent from the product card to a DAC for input into the microactuator controller, which was a simple analog filter. The output of the microactuator controller was sent to an external power amplifier which was used to drive the microactuator in the HDD. For the milliactuator, the control signal was calculated on the product card and then sent to a DAC/driver combination chip. Bipolar drivers were used for both the microactuator and the milliactuator.

A. Microactuator Results

The VCM controller design used in conjunction with the microactuator was very similar to the product design for implementation without the microactuator. The gain was lowered slightly and some modification of the notch filters was made to improve the interaction between the VCM loop and the microactuator loop. Most notable is the addition of a notch filter at the butterfly mode frequency of approximately 6.7 kHz. The result has lower stability margins than the single-stage VCM design, but it is still stable even without the microactuator loop. Fig. 8 shows the open loop frequency responses of the VCM and microactuator loops for the dual-stage system. The handoff region is at approximately 200 Hz. Note that there is minimal destructive interference.

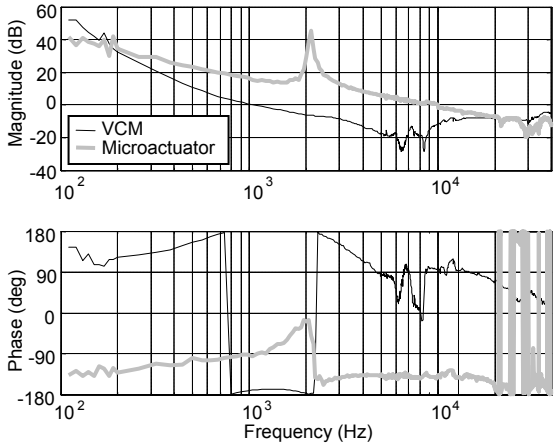

Fig. 8: Open loop frequency responses for the microactuator and VCM dual-stage designs

Fig. 9 shows the open loop frequency response of the VCM-microactuator dual-stage servo, compared with the conventional single-stage VCM servo. The open loop servo bandwidth of the dual-stage system is approximately 8 kHz, with a phase margin of 30 degrees and a gain margin of 5 dB. This is a significant increase compared to the single-stage VCM servo system which has a 1.7 kHz bandwidth for the same stability margins. Fig. 10 shows the error rejection function. The microactuator servo is capable of rejecting error at higher frequency. Note that the resonant peak of the microactuator at 2.2 kHz is lower than the open loop bandwidth and does not pose any stability problems. The high gain at this frequency results in significant disturbance rejection. If the relative position signal is available, the microactuator resonance may be actively damped, as discussed in [4]. Passive damping techniques are also available, as described in [6]. The maximum attainable bandwidth was limited by the sampling rate and not by the mechanics, and the bandwidth can be increased further if the sampling rate is increased.

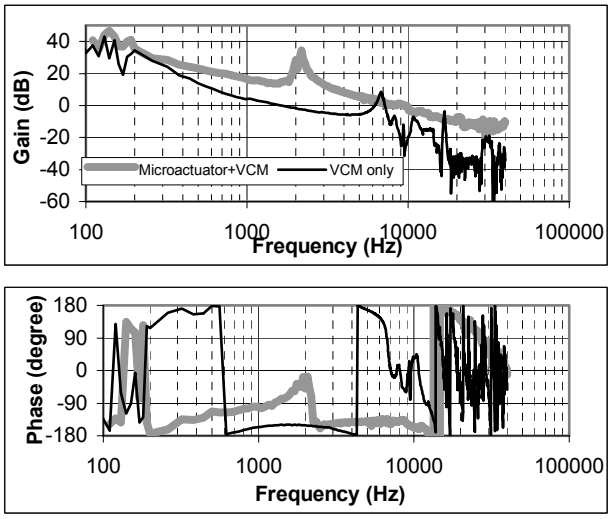

Fig. 9: Open loop frequency responses of the single and dual-stage designs

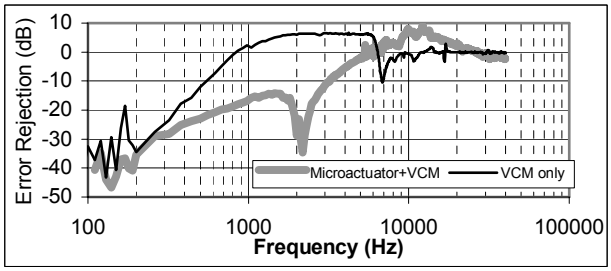

Fig. 10: Error rejection (sensitivity) frequency responses of the single and dual-stage designs

B. Milliactuator Results

One of the aspects of the parallel dual-stage design is that the secondary actuator is supposed to be dominant at frequencies above the handoff frequency. This implies that there must be sufficient "channel separation" between the secondary actuator loop and the VCM loop at high frequencies. One way to achieve this is by notching the higher-frequency mechanical resonances of the VCM. This is the approach that was taken with the design for the microactuator. Unfortunately, this typically results in a reduction of the bandwidth of the VCM loop, or at least its gain at key frequencies, and hence generally a deleterious effect on the stroke required of the secondary actuator. Because of the mechanical differences between the microactuator and the milliactuator, and the resulting difference in controller design strategies, the decreased VCM gain from the notch filters did not affect the microactuator design or its stroke requirements adversely.

An alternative strategy was proposed for the milliactuator where the VCM resonances are allowed to interact with the milliactuator loop at frequencies higher than the handoff frequency. Such a design has to assume more complex and complete models of the VCM and milliactuator. The control design also becomes sensitive to system delays, which have increasing effect on phase change as frequency increases. An example of such a design is shown in Fig. 11. In the figure, the red line represents the VCM loop design and the black line is the overall loop with the milliactuator. It can be seen that there is a low frequency and a high frequency interaction between the two loops. With proper loop-shaping, notching of the VCM mode can be avoided, the VCM loop gain can be kept high, and the required milliactuator stroke can be reduced. The milliactuator is able to achieve a bandwidth of 3.6 kHz with a gain margin of 5 dB and a phase margin of 45 degrees. The phase margin is significantly improved over the single-stage case, resulting in improved disturbance rejection near the crossover frequency.

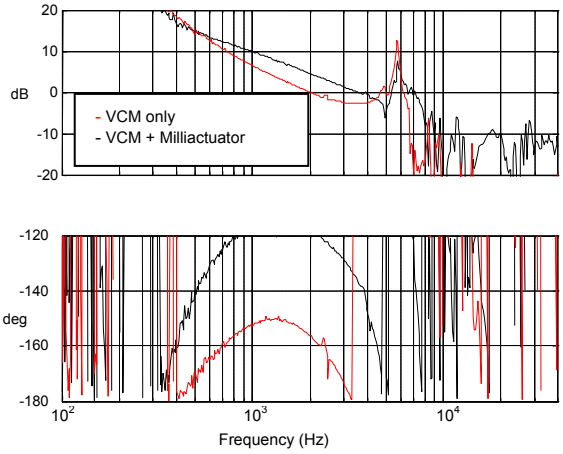

Fig. 11: Higher frequency interaction between the milliactuator and the VCM loop

C. Discussion

The microactuator can be used to achieve higher bandwidth than the milliactuator, due to its clean dynamics between 3 kHz and 100 kHz. However, higher bandwidth does not necessarily translate into improved TMR or track density, especially if the rest of the system cannot be optimized to take advantage of the higher bandwidth. The capacity for higher bandwidth should translate into greater freedom for loop-shaping. However, since the microactuator is limited by the first resonance on how low the bandwidth can be, it takes away some of the loop-shaping freedom. This freedom may be regained through active or passive damping of the microactuator resonance, but at additional cost and complexity.

V. FUTURE DESIGN CONSIDERATIONS

In the past, the system bandwidth has typically been scaled to achieve the desired track density, typically measured in tracks per inch (TPI). However, the addition of a secondary actuator is likely to change the shape of the frequency response and introduce additional resonances and disturbances, so the scaling laws may have to be modified. Since increasing bandwidth does not always increase TPI, a more careful description of track-following capability must be used.

The promise of the secondary actuator as a mid-frequency disturbance attenuator is seen in the sensitivity function shown in Fig. 7 for the example of the milliactuator. This is good news if the disturbance spectrum has significant elements at those frequencies. The increased bandwidth with the secondary actuator also means that the region where the sensitivity function is greater than one is pushed higher in frequency. Unfortunately, this often has an adverse effect in terms of amplifying airflow-induced TMR, which is often at the higher frequencies. Thus, devices like the milliactuator and microactuator warrant careful design of the HDD in terms of airflow-induced disturbances, as do any other techniques which increase the amplification region of the sensitivity function into the airflow-induced disturbance frequencies.

The effect of these disturbances may be particularly problematic if they are associated with actuator resonances that cannot be effectively dealt with by enclosure redesign. Unresolved, this problem may prevent higher-bandwidth systems from providing real benefit to TMR. To address this issue, designs that give servo attenuation at flutter frequencies were explored for both the microactuator and milliactuator. Such a simulation example is shown in Fig. 12 for the milliactuator. The open loop frequency response is shown in red and the resulting sensitivity function is shown in blue, which provides attenuation at the frequencies of interest.

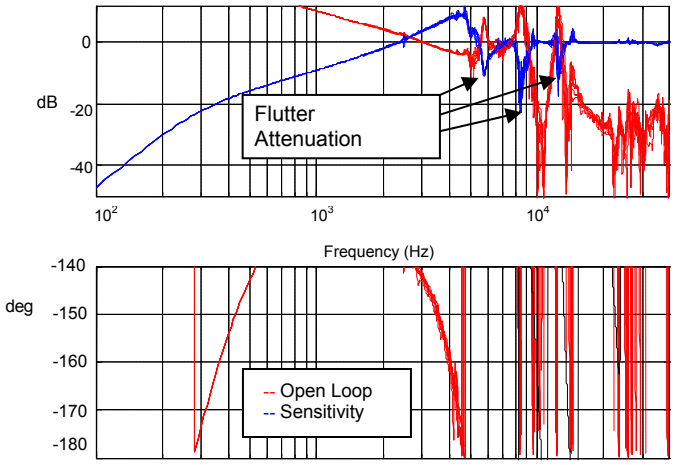

Fig. 12: Flutter attenuation at higher frequencies by loop-shaping

VI. SUMMARY

Two leading candidates for secondary actuation in HDDs were assembled into 10,000 rpm server-class drives. Both were able to achieve significantly higher bandwidth than the standard single-stage actuator, but require different design strategies and pose different trade-offs in terms of manufacturability, integration, and performance.

ACKNOWLEDGMENT

The authors would like to thank Henry Yang, Karen Scott, Harpreet Singh, Surya Pattanaik, Fu-Ying Huang, and Gary Herbst for their efforts on the microactuator manufacturing and file build; and Mike Moser, Kirk Price, Satya Arya, Xin Yang, Bryan Rowan, Jeff Dobbek, Craig Fukushima, and Fred Scott on the milliactuator file build, microcode, and simulations.

REFERENCES

[1] T. Hirano, M. White, H. Yang, K. Scott, S. Pattanaik, S. Arya, F.-Y. Huang, "A Moving-slider MEMS Actuator for High-bandwidth HDD Tracking," *Proc. Intermag*, Anaheim, CA, 2004.

[2] S. Arya, Y.-S. Lee, W.-M. Lu, M. Staudenmann, M. Hatchett, "Piezo-based Milliactuator on a Partially Etched Suspension," *IEEE Trans. Magnetics*, v. 37, n. 2, March 2001, pp. 934-939.

[3] S. Schroeck, W. Messner, "On Controller Design for Linear Time-Invariant Dual-input Single-output Systems," *Proc. Amer. Cntrl. Conf.*, San Diego, CA, 1999, pp. 4122-4126.

[4] M.T. White, T. Hirano, "Use of the Relative Position Signal for Microactuators in Hard Disk Drives," *Proc. Amer. Cntrl. Conf.*, Denver, CO, 2003, pp. 2535-2540.

[5] D. Hernandez, S.-S. Park, R. Horowitz, A. Packard, "Dual-stage Track-following Servo Design for Hard Disk Drives," *Proc. Amer. Cntrl. Conf.,* San Diego, CA, 1999, pp. 4116-4121.

[6] T. Hirano, D. Kercher, M. Mate, "Electrostatic Microactuator with Viscous Liquid Damping," US patent 6,495,944, Dec. 17, 2002.